Hybrid magnon-photon bundle emission from a ferromagnetic-superconducting system

Chengdeng Gou,[1] Xiangming Hu,[1,*] Jun Xu,[1] and Fei Wang[2,†]
[1]*College of Physical Science and Technology, Central China Normal University, Wuhan 430079, People's Republic of China*
[2]*School of Science, Hubei University of Technology, Wuhan 430068, People's Republic of China*

(Received 21 October 2023; revised 18 January 2024; accepted 26 March 2024; published 15 April 2024)

We show that the hybrid magnon-photon bundle emission is possible to generate by employing a three-level Δ-type superconducting artificial atom. The single atom is dispersively coupled with two microwave cavities, one of which simultaneously couples to a yttrium iron garnet (YIG) sphere via the magnetic dipole interaction. Based on the virtual photon exchange, the indirect magnon-atom interaction is established with flexibly tunable coupling strength, thus leading to the consecutive emission of hybrid magnon-photon pairs. The super-Rabi oscillation and Purcell effect make such a hybrid bundle possible in the present three-level system, which is difficult to achieve in the two-level system. The present scheme may find potential applications in quantum information processing and quantum sensing technology.

DOI: 10.1103/PhysRevResearch.6.023052

I. INTRODUCTION

In recent years, the N-photon bundle emission [1], as a peculiar quantum statistical property, has attracted much attention because of its extensive applications in new types of quantum devices such as quantum metrology [2–4], ultrasensitive biosensing [5–7], N-photon sources [8], multiphoton laser [9], and so on. Physically, the bundle emission refers to such a multiphoton process where the N photons are consecutively emitted from a highly excited state, which is prepared by an external pumping field, behaving like a so-called "leapfrog" followed by a relaxing process from the final state to the ground state. In this way, it forms a cycle of N-photon emission where a super-Rabi oscillation is established between the ground state and higher-excited Fock state. From the detection point of view, the behaviors of bundle emission can be described as follows: the photons contained in each bundle are highly correlated while the bundles can be antibunched, uncorrelated, and bunched. The ordinary correlation function is generalized to describe the statistical behaviors of bundle emission. So far, numerous platforms are proposed to realize bundle emission including cavity quantum electrodynamics (QED) [10–16], superconducting microwave resonators [17–21], semiconductor quantum dots (QDs) in microcavities [22,23], waveguide quantum electrodynamics [24], hybrid magnet-qubit systems [25], and so on.

In the typical cavity QED setup [1], the emitter of N-photon bundles is realized under the conditions of the strongly driven two-level system interacting with a detuned cavity mode. Later, spectral filtering of photon emission has been introduced to relax the conditions into the bad-cavity situations [10] and the model is extended to the N-photon Jaynes-Cummings model [15]. The dynamical N-photon bundle emission can be observed in a circuit quantum electrodynamical system driven by two Gaussian-pulse sequences [16]. Differently, relying on an acoustic cavity QED system, an efficient scheme has been studied to generate strongly correlated N phonons (the quanta of mechanical waves) with remarkable advantages of strong robustness, flexible adjustability, and high controllability [11]. Furthermore, motional n-phonon bundle states take place by utilizing the motional degrees of freedom of a trapped atom, which is operated in the currently available parameter regime [23]. Also, the optomechanical systems are suggested to realize the dynamical emission of phonon pairs [13]. Most recently, Yuan *et al.* extended the concept of bundle emission to magnons, in which the similar correlation properties of two or more magnons are studied in a strongly dissipative magnet [25]. Interestingly, the hybrid cavity-magnon system with strong compatibility and scalability provides an ideal platform to construct multi-magnon resources, which are expected to find potential applications in solid-state quantum information processing.

Here, we put forward a new idea to realize a hybrid magnon-photon-pair source by utilizing a hybrid ferromagnet-superconduction quantum system. As is well known, the magnon is defined as quanta of collective spin excitations in magnetic order materials [26,27], in which the yttrium iron garnet (YIG) is a typical representative of constructing hybrid systems with strong coupling [28,29]. Under the excitation of the magnetic field, the emission and transmission of magnons (spin waves) in YIG can be realized through the spin-exchange-induced flow of angular momentum [30,31], which allows information to be carried and propagated at low power. On the one hand, the magnon possesses the unique advantages of high spin density, low dissipation, and flexible tunability. On the other hand, the superconducting circuits can act as an "artificial atom" with discrete levels and have

*xmhu@ccnu.edu.cn.
†feiwang@hbut.edu.cn.

attracted much attention owing to their long coherence time. Specifically, when the mirror symmetry of the effective potential is broken, the Δ-type configuration three-level atom is formed without obeying the optical selection rules between microwave-assisted transitions [32]. In the present scheme, we assume that a microwave cavity simultaneously couples to a three-level Δ-type superconducting atom and a magnon in a dispersive regime. Through the virtual photon exchange, the indirect interaction is established between the magnon and superconducting atom [33]. By driving the atom with an external strong field, the hybrid magnon-photon pair is possible to generate under appropriate conditions. We employ the so-called quantum trajectory method to simulate the emission of a magnon-photon bundle. Our results demonstrate that the antibunched magnon-photon-pair source is generated when the sum frequencies of the photon and magnon are in resonance with the frequency of the dressed-atom transition. Furthermore, we explore how the atomic decay rates assist in realizing a highly correlated magnon-photon-pair source. The present scheme opens up an avenue to investigate the correlation properties between different objects, which may be beneficial to solid-state quantum information processing.

The remaining parts are organized as follows. The model and equations are presented in Sec. II, where all possible spontaneous transitions between the dressed states are analyzed in detail. In Sec. III, the correlation properties are numerically simulated and the intrinsic physical mechanisms are discussed. Furthermore, the super-Rabi oscillation and the role of dissipation in magnon-photon bundle emission are also presented. Finally, a brief conclusion is given in IV.

II. MODEL AND EQUATIONS

Here we use a hybrid ferromagnet-superconductor quantum system to generate hybrid mangon-photon bundle emission. As is shown in Fig. 1(a), a three-level Δ-type superconducting qubit is placed at the intersection of two mutual orthogonal microwave cavities a and b in the x-y plane, and a YIG sphere is installed in the microwave cavity b. The superconducting atom is assumed to be coherently coupled to the two cavities with coupling constants $g_{a,b}$ and driven by an external strong field Ω. Without loss of generality, a biased magnetic field along the z direction is applied to control the frequency of the magnon mode. While the microwave cavity magnetic field is perpendicular to the bias magnetic field and uniform throughout the ferromagnetic crystal, the magnetic dipole coupling vanishes except for the uniform magnetostatic mode, i.e., the Kittel mode [34]. At this time, based on the Holstein-Primakoff approximation [35], the collective spin excitations are approximately represented by the boson operator $m^\dagger$ (m). Then the system Hamiltonian is written as

$$H = H_{ac} + H_{cm}, \tag{1}$$

where the atom-cavity interaction is given by ($\hbar = 1$)

$$\begin{aligned} H_{ac} = &\sum_{j=f,e} \omega_{jg}\sigma_{jj} + \omega_a a^\dagger a + \omega_b b^\dagger b \\ &+ g_a(a\sigma_{fe} + a^\dagger\sigma_{ef}) + g_b(b\sigma_{eg} + b^\dagger\sigma_{ge}) \\ &+ \Omega(\sigma_{fg}e^{-i\omega_l t} + \sigma_{gf}e^{i\omega_l t}), \end{aligned} \tag{2}$$

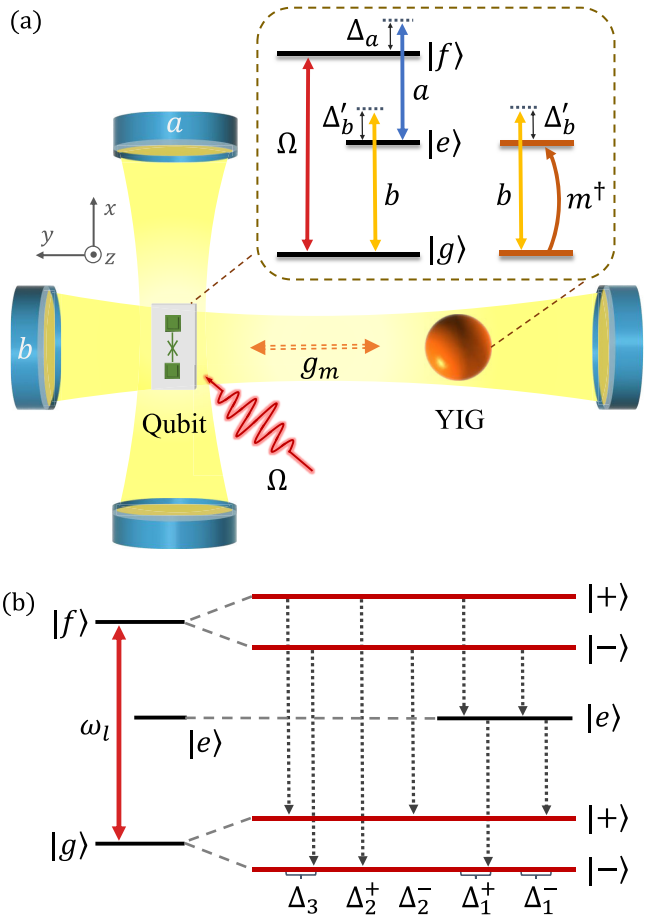

FIG. 1. (a) Schematic representation of the system to generate hybrid magnon-photon bundles. A qubit is placed in the intersection of two mutual orthogonal microwave cavities in the x-y plane, and a YIG sphere is installed on one side of the cavity b. A biased magnetic field is applied in a z direction. Transition $|f\rangle \leftrightarrow |g\rangle$ is driven by a strong microwave field with Rabi frequency Ω, and $|f\rangle \leftrightarrow |e\rangle$ and $|e\rangle \leftrightarrow |g\rangle$ are coupled to two microwave modes a and b, respectively. (b) The possible transitions of the strongly driven qubit in the dressed-state structure.

where a and $a^\dagger$ (b and $b^\dagger$) are the annihilation and creation operators for the cavity mode with frequency ω_a (ω_b). ω_{fg} and ω_{eg} are the transition frequencies between the excited states $|f, e\rangle$ to ground state $|g\rangle$. $\sigma_{ij} = |i\rangle\langle j|$ ($i, j = g, e, f$) represent the projection operators for $i = j$ and the spin-flip operators for $i \neq j$. $g_{a,b}$ are the atom-cavity coupling strengths and Ω is the Rabi frequency of the classical driving field with frequency ω_l. The cavity-magnon interaction Hamiltonian H_{cm} is given by

$$H_{cm} = \omega_m m^\dagger m + g_{bm}(b^\dagger m + b m^\dagger), \tag{3}$$

where g_{bm} desribes the cavity-magnon coupling strength. For simplicity, the Rabi frequency Ω and the coupling constants g_a, g_b, g_{bm} are assumed to be non-negative real numbers.

When the frequency of cavity b is largely detuned from that of the atomic transition $|e\rangle \leftrightarrow |g\rangle$ and magnon mode, and the magnon mode is simultaneously tuned to nearly resonate with transition $|e\rangle \leftrightarrow |g\rangle$, the interaction between the magnon and superconducting atom is established via

the virtual photon exchange. Under an appropriate rotating frame, the total Hamiltonian of the hybrid ferromagnet-superconductor system becomes (see details in Appendix A)

$$\begin{aligned}\tilde{H} =&\Delta_f\sigma_{ff} + \Delta_a a^\dagger a + \Delta_m m^\dagger m + g_a(a\sigma_{fe} + a^\dagger\sigma_{ef})\\ &+ g_m(\sigma_{eg}m + \sigma_{ge}m^\dagger) + \Omega(\sigma_{fg} + \sigma_{gf}),\end{aligned} \tag{4}$$

where we define $\Delta_f = \omega_{fg} - \omega_l$, $\Delta_a = \omega_a - \omega_l + \omega'_{eg}$, $\Delta_m = \omega'_m - \omega'_{eg}$, $g_m = -g_b g_{bm}/\Delta'_b$, with $\omega'_{eg} = \omega_{eg} - g_b^2/\Delta'_b$ and $\omega'_m = \omega_m - g_{bm}^2/\Delta'_b$ being the atom and magnon frequencies including the cavity-induced shift and $\Delta'_b = \omega_b - \omega_{eg}$ being the frequency detuning of the cavity b from the atomic transition $|e\rangle \leftrightarrow |g\rangle$.

The dynamic behaviors of the system are described by the master equation [36,37]

$$\dot{\rho} = -i[\tilde{H}, \rho] + \mathcal{L}_a\rho + \mathcal{L}_c\rho + \mathcal{L}_m\rho, \tag{5}$$

in which the Lindblad terms take the form as

$$\begin{aligned}\mathcal{L}_a\rho =&\frac{\gamma_{fg}}{2}\mathcal{L}[\sigma_{gf}]\rho + \frac{\gamma_{fe}}{2}\mathcal{L}[\sigma_{ef}]\rho + \frac{\gamma_{eg}}{2}\mathcal{L}[\sigma_{ge}]\rho\\ &+ \frac{\gamma_{ff}}{2}\mathcal{L}[\sigma_{ff}]\rho + \frac{\gamma_{ee}}{2}\mathcal{L}[\sigma_{ee}]\rho,\\ \mathcal{L}_c\rho =&\frac{\kappa_a}{2}\mathcal{L}[a]\rho, \quad \mathcal{L}_m\rho = \frac{\kappa_m}{2}\mathcal{L}[m]\rho,\end{aligned} \tag{6}$$

where the damping terms $\mathcal{L}_a\rho$, $\mathcal{L}_c\rho$, $\mathcal{L}_m\rho$ represent the dissipation of the atom, the cavity, and the magnon, respectively. We have $\mathcal{L}[o]\rho = 2o\rho o^\dagger - o^\dagger o\rho - \rho o^\dagger o$. The parameters of γ_{jk} denote the atomic decay rates from state $|j\rangle$ to state $|k\rangle$ and γ_{jj} are pure dephasing rates. The dissipation rates for the cavity a and magnon mode m are represented by κ_a and κ_m, respectively. Generally, the Eq. (5) can be numerically solved by using the QUTIP package in PYTHON [38].

In the strong field limit of $\Omega \gg g_{a,m}$, we can resort to the dressed-state picture to interpret the possible transition channels. By diagonalizing partial Hamiltonian $\tilde{H}_p = \Delta_f\sigma_{ff} + \Omega(\sigma_{fg} + \sigma_{gf})$ under the resonant driving case ($\Delta_f = 0$), the two dressed states are expressed based on two bare-state sublevels $|f\rangle$ and $|g\rangle$ as [39]

$$\begin{aligned}|+\rangle &= \frac{1}{\sqrt{2}}(|g\rangle + |f\rangle),\\ |-\rangle &= \frac{1}{\sqrt{2}}(|g\rangle - |f\rangle).\end{aligned} \tag{7}$$

The two dressed states $|\pm\rangle$ have their eigenvalues of $\varepsilon_\pm = \pm\Omega$ and they are separated by the energy 2Ω ($\hbar = 1$). Correspondingly, the partial Hamiltonian is rewritten as $\tilde{H}_p = \Omega(\sigma_{++} - \sigma_{--})$, where σ_{jk} ($j, k = +, -, e$) are projection operators for $j = k$ or spin-flip operators for $j \neq k$. According to the dressed-state basis, the possible spontaneous transition channels and corresponding frequency conditions are given by

$$\left.\begin{aligned}|\pm\rangle &\to |e\rangle\\ |e\rangle &\to |\mp\rangle\end{aligned}\right\}: \quad \Delta_1^\pm = \pm\Omega, \tag{8}$$

$$|\pm\rangle \to |\mp\rangle: \quad \Delta_2^\pm = \pm 2\Omega, \tag{9}$$

$$|\pm\rangle \to |\pm\rangle: \quad \Delta_3 = 0. \tag{10}$$

The above transitions are sketched in Fig. 1(b). For the atomic transition $|f\rangle \leftrightarrow |g\rangle$, the central peak is expected to occur at $\omega = \omega_{fg}$, accompanied by two symmetric outer sidebands at $\omega = \omega_{fg} \pm 2\Omega$. Besides, there is a pair of inner sidebands at $\omega = \omega_{fg} - \omega'_{eg} \pm \Omega$ (or $\omega = \omega'_{eg} \pm \Omega$) for transition $|f\rangle \leftrightarrow |e\rangle$ (or $|e\rangle \leftrightarrow |g\rangle$). By choosing appropriate detuning, the excitation of single photons (magnons) happens between the bare state $|e\rangle$ and dressed states $|\pm\rangle$ shown in Eq. (8). We note that this scheme differs from conventional two-level systems due to the existence of the bare state $|e\rangle$. Intriguingly, the hybrid magnon-photon pair emission is possible to obtain through the transitions in Eqs. (9), (10), and $|e\rangle \to |e\rangle$, which can be seen from Eq. (A11). The validity of the theoretical analysis is confirmed through the numerical simulation presented below.

III. NUMERICAL RESULTS AND DISCUSSIONS

In this section, we mainly investigate the generation of antibunched magnon-photon bundle emission by numerical calculations. Moreover, the super-Rabi oscillation and the intrinsic physical mechanisms are analyzed in terms of the dressed-state picture. The dissipation effects on the hybrid bundle emission are also discussed.

A. Evidence of hybrid magnon-photon bundle

First, we would like to demonstrate the generation of hybrid magnon-photon bundle emission. For the general Mollow triplet [40], the multiphoton processes are typically concealed beneath the single-photon processes since the higher-order nonlinear effects are extremely weak. Nevertheless, such processes can be exploited when the following conditions are satisfied, i.e., the emission of N identical photons in a cavity is resonant with the dressed-state transition [41]. At this time, the multiphoton processes are enhanced due to the Purcell effects, leading to the generation of N-photon bundle emission [1]. Differently, in our work, we consider a special resonant condition of $p\Delta_a + q\Delta_m = \Delta_1^\pm, \Delta_2^\pm, \Delta_3$, where p and q are non-negative integers. This resonant condition allows us to observe the hybrid magnon-photon bundle emission with different frequencies of magnons and photons, where the sum of frequencies for p photons and q magnons equals the frequency of the dressed-state transition. This frequency matching condition can be satisfied by choosing proper frequencies with the help of state $|e\rangle$ but is hard to meet in the normal two-level system. Taking $(\Delta_a, \Delta_m) = (2\Omega, 0)$ as an example, we show the emission spectrum $\int d\tau \langle o^\dagger(0)o(\tau)\rangle e^{i\omega\tau}$ ($o = a, m$) in Fig. 2. Without loss of generality, we always choose $g_a = g_m = g$ and $\kappa_a = \kappa_m = \kappa$ throughout the paper. The parameters are chosen as $\Omega = 20g$, $\gamma_{fg} = 0.02g$, $\gamma_{fe} = 0.01g$, $\gamma_{eg} = 0.012g$, $\gamma_{ff} = \gamma_{ee} = 0.005g$, $\kappa = 0.2g$, and $\Delta_f = 0$. The single-photon (or single-magnon) processes are observed at $\omega_{fg} - \omega'_{eg} \pm \Omega$ (or $\omega'_{eg} \pm \Omega$), and the cascade magnon-photon emission (labeled by A) appears at $\omega_{fg} - \omega'_{eg} + 2\Omega$ for cavity a and at ω'_{eg} for magnon m. Here, the magnon frequency refers to ω'_m that includes the cavity-induced shift. It is evident that the peaks labeled by A are much higher than others due to the Purcell enhancement by the cavity and the magnon. Notably, the emissions of photons and magnons in the cascade transition are not independent events because they are far from the single-quantum resonant transitions in the dressed-states basis.

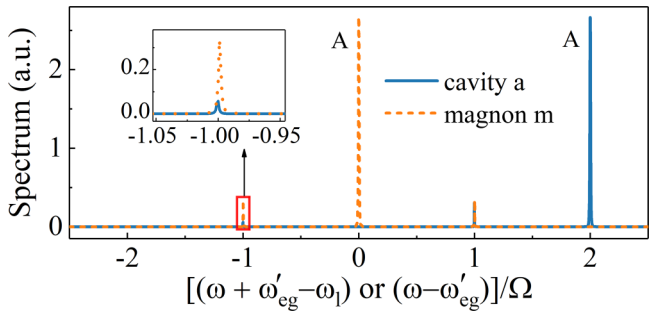

FIG. 2. Emission spectrum as a function of $(\omega + \omega'_{eg} - \omega_l)/\Omega$ for cavity a and of $(\omega - \omega'_{eg})/\Omega$ for magnon m. The parameters here are $\Omega = 20g$, $\gamma_{fg} = 0.02g$, $\gamma_{fe} = 0.01g$, $\gamma_{eg} = 0.012g$, $\gamma_{ff} = \gamma_{ee} = 0.005g$, $\kappa = 0.2g$, $\Delta_a = 2\Omega$, $\Delta_m = 0$, and $\Delta_f = 0$.

To describe the hybrid magnon-photon emission as mentioned above, we introduce the time-delayed second-order correlation functions as defined in Ref. [42]

$$g^{(2)}_{\alpha\beta}(\tau) = \frac{\langle \alpha^\dagger(0)\beta^\dagger(\tau)\beta(\tau)\alpha(0)\rangle}{\langle \alpha^\dagger\alpha(0)\rangle\langle\beta^\dagger\beta(\tau)\rangle}, \tag{11}$$

where $g^{(2)}_{\alpha\beta}(\tau)$ $(\alpha, \beta = a, m)$ represent the autocorrelation functions for $\alpha = \beta$ while the cross-correlation function for $\alpha \neq \beta$. When $\tau = 0$, $g^{(2)}_{\alpha\beta}(\tau)$ denote the equal-time second-order correlation functions. As defined, the bunching effect happens when the condition of $g^{(2)}_{\alpha\beta}(0) > g^{(2)}_{\alpha\beta}(\tau)$ (or $g^{(2)}_{\alpha\beta}(0) > 1$) holds, and its stationary statistics are super-Poisson distribution. Otherwise, the stationary statistics are characterized by a sub-Poisson distribution when $g^{(2)}_{\alpha\beta}(0) < 1$ and have an antibunching effect. These functions can be numerically simulated by solving the master equation (5) within a truncated Hilbert space.

Figure 3(a) displays the density plot of the logarithm of equal-time second-order cross-correlation function $g^{(2)}_{am}(0)$ as a function of the detuning Δ_a and Δ_m. In this contour, the dark areas denote the strong cross-correlation effects for $g^{(2)}_{am}(0) \gg 1$, corresponding to superbunching behaviors. Interestingly, we observe that the superbunching peaks at $\Delta_a + \Delta_m = \Delta_2^{\pm}, \Delta_3$ are suddenly changed into superbunching dips. To show it clearly, we plot the autocorrelations $g^{(2)}_{aa}(0)$, $g^{(2)}_{mm}(0)$, and cross-correlation $g^{(2)}_{am}(0)$ as functions of Δ_a in Fig. 3(b), while setting $\Delta_m = 0$. The superbunching dips of $g^{(2)}_{am}(0)$

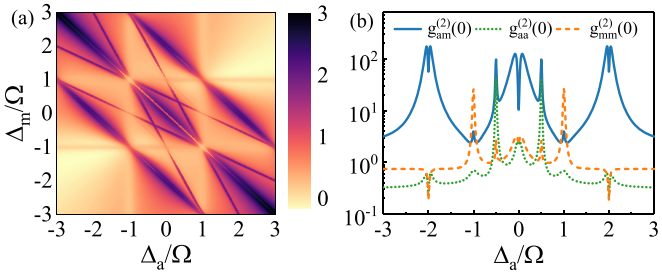

FIG. 3. (a) The logarithm of equal-time second-order cross-correlation function $g^{(2)}_{am}(0)$ as a function of the detuning Δ_a/Ω and Δ_m/Ω. (b) The equal-time second-order cross- and auto-correlation function $g^{(2)}_{\alpha\beta}(0)$, $(\alpha\beta = am, aa, mm)$ as functions of Δ_a/Ω with $\Delta_m = 0$. The other parameters are the same as those in Fig. 2.

appear at the central peak and two outer sidebands, implying the occurrence of bundle emission [1]. Furthermore, we find that the two autocorrelations $g^{(2)}_{aa}(0)$ and $g^{(2)}_{mm}(0)$ are antibunching at $\Delta_a = \pm 2\Omega$ while bunching at $\Delta_a = 0$, which indicate the different statistics of pair emission. Similar to the studies in Refs. [43,44], correlated magnon-photon laser may occur at $\Delta_a = 0$. Here, we mainly focus on the photon emissions at $\Delta_a = \pm 2\Omega$, which exhibit much stronger nonclassical statistics [45]. In the following, we will demonstrate the emergence of antibunched hybrid magnon-photon bundles and analyze their intrinsic mechanisms.

B. Analysis of super-Rabi oscillation

According to the above discussions, we note that the properties of the emitted hybrid magnon-photon bundle can be understood based on the correlation functions. To gain a deeper understanding of the intrinsic mechanisms involved, we would like to analyze the super-Rabi oscillations as proposed in [1]. As is well known, super-Rabi oscillation plays a pivotal role in the generation of bundle emission. In our scheme, we consider the specific example of $(\Delta_a, \Delta_m) = (2\Omega, 0)$. At this time, the sum of frequencies of the emitted magnons and photons is equal to the transition frequency from the dressed state $|+\rangle$ to state $|-\rangle$. According to Eq. (A13), the effective interaction Hamiltonian, under resonant driving condition $\Delta_f = 0$, is derived as

$$\begin{aligned} H^I_{\rm eff} &= -\frac{1}{2\Omega} g_a g_m \sigma_{+-} am + \text{H.c.} \\ &= \sum_{p,q=0}^{\infty} g^{p,q}_{\rm eff} |p, q, +\rangle\langle p+1, q+1, -| + \text{H.c.}, \end{aligned} \tag{12}$$

where the effective super-Rabi frequency is defined as $g^{p,q}_{\rm eff} = -g_a g_m \sqrt{(p+1)(q+1)}/2\Omega$. The direct product state $|p, q, j\rangle = |p\rangle \otimes |q\rangle \otimes |j\rangle$ denotes the state with photon occupancy $|p\rangle$, the magnon occupancy $|q\rangle$ when the atom stays in the state $|j\rangle$. The interaction Hamiltonian describes the physical process in which the dressed transition from state $|+\rangle$ to $|-\rangle$ (or $|-\rangle$ to $|+\rangle$) is accompanied by the successive emission (or absorption) of a photon and a magnon, thereby termed as super-Rabi oscillation. When the system is initially prepared in state $|0, 0, +\rangle$, i.e., the cavity and magnon are in a vacuum state and the atom is in state $|+\rangle$, the system will oscillate back and forth between states $|0, 0, +\rangle$ and $|1, 1, -\rangle$, while the other transitions are inhibited. In Fig. 4, we numerically plot the time-evolution of state populations P_{00+} and P_{11-}, neglecting the dissipation effects temporarily. Here, $P_{pqj} = |\langle p, q, j|\psi(t)\rangle|^2$. The solid line and the "dot" symbol represent P_{00+} while the dashed line and the "'triangle" symbol denote P_{11-}. Obviously, the perfect super-Rabi oscillation occurs, which aligns well with the theoretical analysis.

C. Dissipation triggered the hybrid magnon-photon bundle emission

In Fig. 4, we simulate the ideal super-Rabi oscillation without considering the environmental noises. However, in realistic situations, the dissipation effects must be included since the system is usually bathed in different environments.

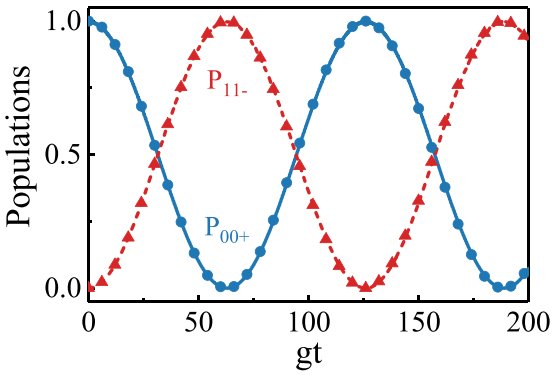

FIG. 4. Time evolution of the state popultions P_{00+} and P_{11-} without the dissipation at two-quantum resonance $(\Delta_a, \Delta_m) = (2\Omega, 0)$. The solid and dashed lines are plotted by using the original Hamiltonian Eq. (4), and the circular and triangular points are plotted by using the effective Hamiltonian Eq. (12). The initial state is in $|0, 0, +\rangle$, and other parameters are $\Omega = 20g$ and $\Delta_f = 0$.

In this section, we investigate a case where the bundle emission is affected by the magnon dissipation, cavity dissipation, and atomic decay rates. To characterize the whole process of the bundle emission, we use Monte Carlo simulation to record the individual trajectory of the system. In Figs. 5(a) to 5(c), the dynamical evolutions of the populations P_{pqj} are plotted in the presence of dissipation effect at $\Delta_a = 2\Omega$, $\Delta_m = 0$. It is assumed that the system is initially located in the state $|0, 0, +\rangle$, i.e., the cavity mode and the magnon mode are in the vacuum states and the atom is in the dressed state $|+\rangle$. As seen in Fig. 5(c), the system is initially pumped into the target state of $|1, 1, -\rangle$ from its initial state $|0, 0, +\rangle$ with the probability of 0.015 at $\kappa t = 4.2$. During this process, other transitions, including the one-photon and two-photon processes, are greatly suppressed. When the system undergoes

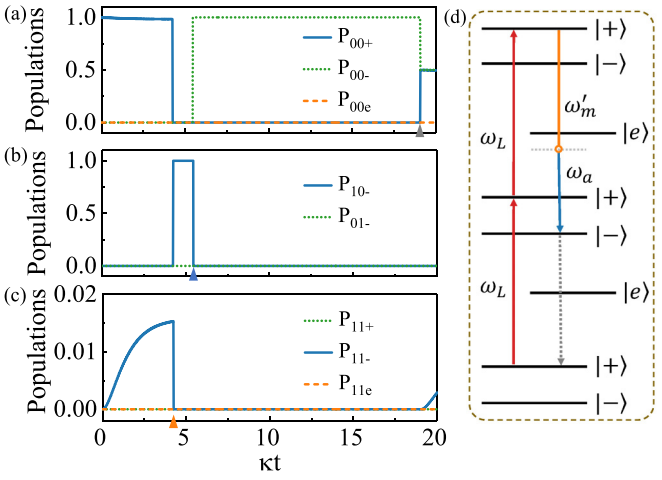

FIG. 5. (a)–(c) Quantum trajectories for the hybrid magnon-photon emission in the presence of system dissipation. The lines represent the dynamics of the state population P_{nmj}. The parameters are the same as those in Fig. 2. (d) The hybrid magnon-photon bundle emission in dressed states. The yellow-blue arrow indicates the Purcell-enhanced magnon-photon transition and the dashed arrow represents the spontaneous emission of the atom.

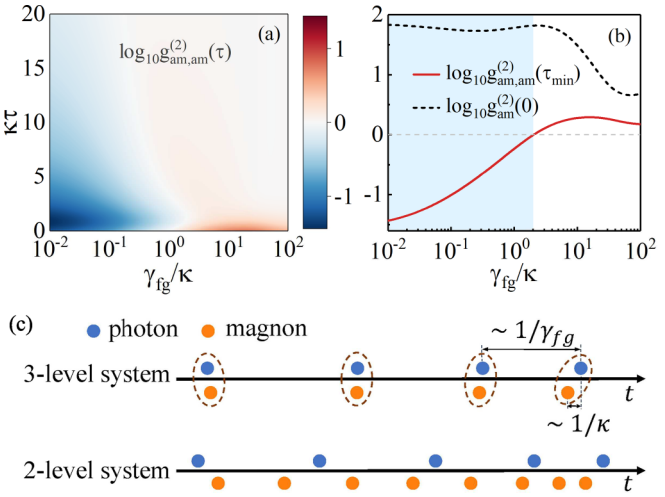

FIG. 6. (a) Logarithmic plot of time-delayed generalized correlation function $g^{(2)}_{am,am}(\tau)$ as a function of relative rates γ_{fg}/κ. (b) Logarithmic plot of $g^{(2)}_{am,am}(\tau_{\min})$ and $g^{(2)}_{am}(0)$ as functions of γ_{fg}/κ. The parameters are the same as those in Fig. 2. (c) The detection of magnon and photon emissions from the hybrid system by placing a three-level system and two-level system into the cavity, respectively, wherein the blue point represents photon and yellow point magnon. The first time axis indicates that the hybrid bundle emission is generated while the second one demonstrates that the events of magnon emission and photon emission are random.

a quantum collapse triggered by dissipation, a single magnon is emitted, resulting in a transition to the single-photon state $|1, 0, -\rangle$ with a probability close to unity [see the solid line from Fig. 5(b)]. Owing to the strong correlation effects between magnon and photon, a photon is subsequently emitted from cavity a and the quantum state evolves into $|0, 0, -\rangle$, completing the emission of a hybrid magnon-photon bundle. For clarity, the emission event of a magnon is denoted by a yellow triangle in Fig. 5(c) while the emission of a photon is indicated by a blue triangle in Fig. 5(b). Notably, the quantum state $|0, 0, -\rangle$ returns to the initial state when the atomic dressed state is flipped from state $|-\rangle$ to state $|+\rangle$, as shown in Fig. 5(d), which is denoted by the gray triangle in Fig. 5(a). In the final step, a photon will be emitted from the flip without affecting the bundle emission due to its different frequency. According to the above analysis, the cycle process is formed, which enables the successive bundle emissions. It appears that the magnon is emitted followed by a strongly correlated photon, as shown in Fig. 5. Nevertheless, this sequence can be reversed, i.e., the magnon can be emitted from the system after a photon, which is sketched in Fig. 6(c). This means that the correlation between magnon and photon is symmetric [see Fig. 8(a)] and the emitted photon can herald the presence of a magnon, or vice versa, within a bundle. Furthermore, we introduce the generalized second-order correlation function to describe such a hybrid bundle emission [1,41]

$$g^{(2)}_{am,am}(\tau) = \frac{\langle (am)^\dagger(0)(am)^\dagger(\tau)(am)(\tau)(am)(0)\rangle}{\langle (am)^\dagger(am)(0)\rangle \langle (am)^\dagger(am)(\tau)\rangle}, \qquad (13)$$

where $|\tau| \geqslant \tau_{\min} = 1/\kappa$. $\tau_{\min}$ can be approximately regarded as zero-time delay since the probe is inside bundle itself within the cavity (magnon) lifetime $1/k$.

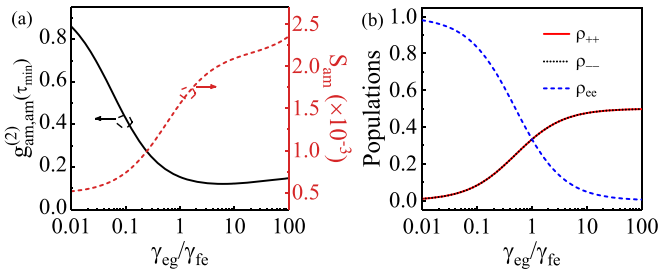

FIG. 7. (a) The zero-time delayed generalized correlation function $g^{(2)}_{am,am}(\tau_{\min})$ and the bundle emission rate S_{am} as functions of γ_{eg}/γ_{fe}. (b) Dressed populations as functions of γ_{eg}/γ_{fe}. The parameters are the same as those in Fig. 2.

In Fig. 6(a), the time-delayed generalized correlation function $g^{(2)}_{am,am}(\tau)$ as a function of ratio γ_{fg}/κ is plotted. From this figure, it is found that $g^{(2)}_{am,am}(\tau)$ evolves from bunching into antibunching as the ratio of γ_{fg}/κ is decreased, passing by the coherent emission with $g^{(2)}_{am,am}(\tau) = 1$. The long-lived atom guarantees that the timescale between the hybrid bundle emission is much longer than the time interval between the magnon and photon in a bundle, giving rise to the appearance of antibunched hybrid magnon-photon bundles. To show it clearly, we plot the zero-time delayed $g^{(2)}_{am,am}(\tau_{\min})$ (solid line) and $g^{(2)}_{am}(0)$ (dashed line) versus γ_{fg}/κ in Fig. 6(b). When $\gamma_{fg} < 2\kappa$, we have $g^{(2)}_{am}(0) > 1$ and $g^{(2)}_{am,am}(\tau_{\min}) < 1$, which implies the occurrence of antibunched hybrid bundle emission in the shaded region. Otherwise, the bundle antibunching disappears in the region of $\gamma_{fe} > 2\kappa$ because of $g^{(2)}_{am}(0) > 1$ and $g^{(2)}_{am,am}(\tau_{\min}) \geqslant 1$. The emissions of the antibunched hybrid magnon-photon bundle are sketched in Fig. 6(c), where the emitted magnons are denoted by yellow circles below the time axis, and the photons are represented by blue circles above it. For the present three-level system, when a magnon arrives at a certain time, it is possible to detect a correlated photon at approximately the same time. The system behaves as an antibunched magnon-photon-pair emitter since the time interval $1/\gamma_{fg}$ between the consecutive pulses is much larger than the time $1/\kappa$ in a bundle. For comparison, we also draw the emissions of magnons and photons in the two-level system, where the atomic transition simultaneously couples to the magnon, the cavity, and the strong driving field. It shows that the

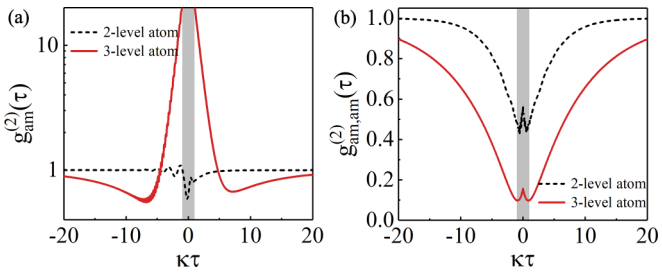

FIG. 8. (a) The time-delayed cross-correlation function $g^{(2)}_{am}(\tau)$ and (b) the time-delayed generalized correlation functions $g^{(2)}_{am,am}(\tau)$ for two-level and three-level case. We choose $g_a = g_m = g$, $\kappa_a = \kappa_m = 0.2g$, $\gamma = 0.02g$, $\Omega = 20g$, $\Delta_f = 0$, and $(\Delta_a, \Delta_m) = (2\Omega, 0)$ in two-level case. For the three-level case, the parameters are the same as those in Fig. 2.

emitted photons and magnons are random since there is no strong correlation effect between them [see Fig. 8(a)]. Therefore, the three-level system is a good candidate for producing hybrid magnon-photon bundles. In addition, we define a parameter of emission rate $S_{am} = \kappa\bar{n}/g$ to describe the quantity of the bundle emission, where $\bar{n}$ is the mean magnon-photon number of magnon m and cavity a. To do so, we plot the correlation function $g^{(2)}_{am,am}(\tau_{\min})$ (black solid line) and emission rate S_{am} (red dashed line) as functions of the relative atomic decay rate γ_{eg}/γ_{fe}. In the range of $0.01 < \gamma_{eg}/\gamma_{fe} < 100$, there is $g^{(2)}_{am,am}(\tau_{\min}) < 1$, which indicates the antibunching effects of bundle emission. With the increasing of γ_{eg}/γ_{fe}, the correlation function $g^{(2)}_{am,am}(\tau_{\min})$ falls sharply at first and finally approaches a stable value. On the other hand, the variation trend for emission rate is opposite to that of the correlation function. This indicates that a large-quantity magnon-photon-pair resource is possible to acquire by choosing an appropriate value of γ_{eg}/γ_{fe}. Physically, this can be understood based on the dressed-state population, which is shown in Fig. 7(b). As the ratio γ_{eg}/γ_{fe} is increased, the dressed population ρ_{ee} decreases gradually while $\rho_{\pm\pm}$ is increased. The population inversion occurs at a point of $\gamma_{eg}/\gamma_{fe} = 1$. The enhancement of populations $\rho_{\pm\pm}$ results in a higher emission rate S_{am}. In addition, the decay rates from $|\pm\rangle \to |e\rangle$ or $|e\rangle \to |\pm\rangle$ given in Appendix B are determined by the ratio γ_{eg}/γ_{fe}.

To emphasize the main advantages of the present scheme compared with the 2-level system, in Fig. 8, we plot the time-delayed correlation functions $g^{(2)}_{am}(\tau)$ and $g^{(2)}_{am,am}(\tau)$ in two cases, respectively. The first represents the correlation between magnon and photon within a bundle, and the second denotes the correlation of a hybrid bundle with the adjacent one. For simplicity, the calculation procedure is not given here because it is similar to the present work. The parameters of the two-level case are the same as those in the three-level system. The antibunched hybrid bundle emission is possible to generate if and only if the following conditions are satisfied: $g^{(2)}_{am}(0) > g^{(2)}_{am}(\tau)$ and $g^{(2)}_{am,am}(0) < g^{(2)}_{am,am}(\tau)$. As shown in Fig. 8(a), the features of the correlation function of $g^{(2)}_{am}(\tau)$ are summarized as follows. On the one hand, the correlation function in the three-level system is nearly symmetrical about zero time, which is asymmetrical in the two-level system. On the other hand, it is much larger than unity in certain time domains (shadowed in gray), indicating a strong correlation between magnon and photon. However, in the two-level system, the correlation function is always smaller than or close to unity, implying the absence of bunching behaviors between magnon and photon. This also can be observed in Fig. 6(c). Furthermore, we note that the antibunching effects between the bundles in the three-level system are more obvious than those of in the two-level system. In brief, the hybrid magnon-photon bundle emission is possible to attain in the three-level system, but is difficult for the two-level system.

Before ending this section, we briefly discuss the feasibility of the experimental scheme. As illustrated in Fig. 1, our system contains two microwave cavities, a superconducting artificial atom, and an undoped single-crystal YIG sphere, positioned in the x-y plane. The superconducting artificial atom is located at the intersection (near the maximum electric fields) of the cavities, and the YIG sphere is installed in one

cavity (near the antinode of the magnetic field). In our work, the two microwave cavities can be fabricated in a planar cross-shaped cavity or coplanar waveguide [46,47], which allows for flexible adjusting to far-detuned from the atom and the magnon mode. At the same time, the dissipation rate of cavity b should keep large enough to satisfy the effective coherent coupling effect between the atom and magnon. In addition, owing to the high spin density of YIG, experimental achievements have demonstrated strong coupling even ultra-strong coupling between magnons and microwave photons [48–55], which guarantee the realization of a strong coupling between the magnon mode and the artificial atom [33,56]. Such advantages are not only beneficial for correlated magnon-photon emission in our scheme but also for other related research [57–62]. Experimentally, the emission of magnons in YIG can be detected by performing state tomography to analyze the density matrix of its magnetization dynamical states [63,64]. On the other hand, one can read out the magnon states by coupling the magnon to another superconducting qubit in a strong dispersive regime [65,66]. Benefiting the advantage of the strong correlation between photons and magnons within a bundle, our scheme provides a promising candidate for probing the single-magnon emissions by detecting the photons.

IV. CONCLUSION

In conclusion, we proposed a novel scheme to generate hybrid magnon-photon bundles from a three-level Δ-type artificial atom in a ferromagnetic-superconducting system. By applying a microwave cavity simultaneously couples to one of the atomic transitions and the magnon in the dispersive regime, the interaction between the magnon and atom is established via the virtual photon exchange while the other cascade transition is directly coupled with the other microwave cavity. Then the cascade emission of the correlated photon pair is replaced by a hybrid magnon-photon pair. With a strong driving field to excite the system into a target state, the super-Rabi oscillation is formed between the excited state and the initial state. As a consequence, the antibunched hybrid magnon-photon bundle is possible to obtain when the atomic lifetime is much longer than that of the cavity and magnon mode. We also numerically simulate various correlation functions to describe the statistical properties of the hybrid bundle emission and the intrinsic physical mechanisms are analyzed based on the dressed-state picture. The present scheme offers a promising avenue for preparing hybrid bundle emissions, which is expected to find potential applications in quantum information processing and quantum sensing technology.

ACKNOWLEDGMENTS

This work is supported by the National Natural Science Foundation of China (Grants No. 12274164, No. 12375011, and No. 61875067).

APPENDIX A: DERIVATION OF EFFECTIVE HAMILTONIAN

We first present the detailed derivation for Eq. (4). In the rotating frame of $H' = \omega_l(\sigma_{ff} + a^\dagger a) + \omega_{eg}(\sigma_{ee} - a^\dagger a + b^\dagger b + m^\dagger m)$, the original Hamiltonian is written as

$$\begin{aligned} H =&\Delta_f\sigma_{ff} + \Delta_a' a^\dagger a + \Delta_b' b^\dagger b + \Delta_m' m^\dagger m \\ &+ g_a(a\sigma_{fe} + a^\dagger\sigma_{ef}) + g_b(b\sigma_{eg} + b^\dagger\sigma_{ge}) \\ &+ g_{bm}(b^\dagger m + bm^\dagger) + \Omega(\sigma_{fg} + \sigma_{gf}), \end{aligned} \tag{A1}$$

in which the detunings are defined as $\Delta_f = \omega_{fg} - \omega_l$, $\Delta_a' = \omega_a - \omega_l + \omega_{eg}$, $\Delta_b' = \omega_b - \omega_{eg}$, and $\Delta_m' = \omega_m - \omega_{eg}$. Thus, the dynamics of the cavity b are governed by the following Langevin equations:

$$\dot{b} = -i\Delta_b' b - ig_b\sigma_{ge} - ig_{bm}m, \tag{A2}$$

$$\dot{m} = -i\Delta_m' m - ig_{bm}b, \tag{A3}$$

$$\dot{\sigma}_{ge} = -ig_a a^\dagger\sigma_{gf} + ig_b(\sigma_{ee} - \sigma_{gg})b + i\Omega\sigma_{fe}. \tag{A4}$$

In the large detuning limit, i.e., $\Delta_b' \gg \Omega, \Delta_m', g_b, g_{bm}$, the cavity mode b is adiabatically eliminated by setting $\dot{b} = 0$. The steady-state solution for mode b is

$$b = -\frac{1}{\Delta_b'}(g_b\sigma_{ge} + g_{bm}m), \tag{A5}$$

which is substituted into Eqs. (A3) and (A4). In the second rotating frame of $-\frac{g_b^2}{\Delta_b'}(\sigma_{ee} + m^\dagger m - a^\dagger a)$, the Hamiltonian is given by

$$\begin{aligned} \tilde{H} =&\Delta_f\sigma_{ff} + \Delta_a a^\dagger a + \Delta_m m^\dagger m + g_a(a\sigma_{fe} + a^\dagger\sigma_{ef}) \\ &+ g_m(\sigma_{eg}m + \sigma_{ge}m^\dagger) + \Omega(\sigma_{fg} + \sigma_{gf}), \end{aligned} \tag{A6}$$

where $\Delta_a = \Delta_a' - g_b^2/\Delta_b'$, $\Delta_m = \Delta_m' + (g_b^2 - g_{bm}^2)/\Delta_b'$, and $g_m = -g_b g_{bm}/\Delta_b'$.

In the next, we derive the effective Hamiltonian (12) in the general case. In the dressed-state picture, the total Hamiltonian of the atom-cavity coupling system is expressed as $\tilde{H} = H_0 + V$, where

$$H_0 = \Delta_a a^\dagger a + \Delta_m m^\dagger m + \varepsilon_+\sigma_{++} + \varepsilon_-\sigma_{--}, \tag{A7}$$

$$V = g_a a(c\sigma_{+e} - s\sigma_{-e}) + g_m m(s\sigma_{e+} + c\sigma_{e-}) + \text{H.c.}, \tag{A8}$$

where $c = [\varepsilon_+/\bar{\Omega}]^{1/2}$, $s = [-\varepsilon_-/\bar{\Omega}]^{1/2}$, and $\varepsilon_\pm = (\Delta_f \pm \bar{\Omega})/2$ with $\bar{\Omega} = \sqrt{\Delta_f^2 + 4\Omega^2}$. Then an effective Hamiltonian can be obtained by applying a unitary transformation $H_{\text{eff}} = \exp(-\lambda S)H\exp(\lambda S)$, where we introduce a non-Hermitian operator

$$\begin{aligned} S =&\frac{g_a c}{\Delta_a - \varepsilon_+}a\sigma_{+e} - \frac{g_a s}{\Delta_a - \varepsilon_-}a\sigma_{-e} + \frac{g_m s}{\Delta_m + \varepsilon_+}m\sigma_{e+} \\ &+ \frac{g_m c}{\Delta_m + \varepsilon_-}m\sigma_{e-} - \text{H.c.}, \end{aligned} \tag{A9}$$

with the satisfaction of $V + [H_0, S] = 0$. The parameter λ is introduced to represent the degree of perturbation and V is rewritten as λV. In terms of the Baker-Campbell-Hausdorff formula, we expand H_{eff} to second-order in λ

$$\begin{aligned} H_{\text{eff}} =&H_0 + \lambda V - \lambda[S, H_0] - \lambda^2[S, V] \\ &+ \frac{\lambda^2}{2!}[S, [S, H_0]] + O(\lambda^3) \\ =&H_0 - \frac{\lambda^2}{2}[S, V] + O(\lambda^3). \end{aligned} \tag{A10}$$

By setting $\lambda = 1$, the effective interaction Hamiltonian is obtained as

$$H_{\rm eff}^{I} = \tfrac{1}{2} g_a g_m am[\eta_{+-}\sigma_{+-} + \eta_{-+}\sigma_{-+} + \eta_{++}\sigma_{++} + \eta_{--}\sigma_{--} + \eta_{ee}\sigma_{ee}] + \text{H.c.}, \tag{A11}$$

with

$$\begin{aligned}
\eta_{+-} &= -c^2\left(\frac{1}{\Delta_a - \varepsilon_+} - \frac{1}{\Delta_m + \varepsilon_-}\right),\\
\eta_{-+} &= s^2\left(\frac{1}{\Delta_a - \varepsilon_-} - \frac{1}{\Delta_m + \varepsilon_+}\right),\\
\eta_{++} &= -cs\left(\frac{1}{\Delta_a - \varepsilon_+} - \frac{1}{\Delta_m + \varepsilon_+}\right),\\
\eta_{--} &= cs\left(\frac{1}{\Delta_a - \varepsilon_-} - \frac{1}{\Delta_m + \varepsilon_-}\right),\\
\eta_{ee} &= cs\left(\frac{1}{\Delta_a - \varepsilon_+} - \frac{1}{\Delta_a - \varepsilon_-} - \frac{1}{\Delta_m + \varepsilon_+} + \frac{1}{\Delta_m + \varepsilon_-}\right).
\end{aligned} \tag{A12}$$

Equation (A11) reveals that the transition between atomic dressed states is accompanied by the absorption or emission of both a magnon and a photon. When driving the system to the two-quantum resonance, i.e., $\Delta_a + \Delta_m = \varepsilon_+ - \varepsilon_-$, the effective interaction Hamiltonian can be simplified as

$$H_{\rm eff}^{I} = \tfrac{1}{2} g_a g_m \eta_{+-}\sigma_{+-} am + \text{H.c.} \tag{A13}$$

APPENDIX B: DRESSED ATOMIC POPULATION

In the dressed basis, the master equation is given by

$$\begin{aligned}
\dot{\rho} = &-i[H_0 + V, \rho] + \frac{\kappa_a}{2}\mathcal{L}[a]\rho + \frac{\kappa_m}{2}\mathcal{L}[m]\rho\\
&+ \sum_{i,j=+,e,-} \Gamma_{ij}\mathcal{L}[\sigma_{ji}]\rho + \Gamma_1^{\rm in}\sum_{i,j=+,-}^{i\neq j}\sigma_{ie}\rho\sigma_{ej}\\
&- \Gamma_2^{\rm in}\sum_{i,j=+,-}^{i\neq j}\left(\sigma_{ei}\rho\sigma_{je} - \frac{1}{2}\sigma_{ij}\rho - \frac{1}{2}\rho\sigma_{ij}\right)\\
&+ \Gamma_1^{\rm ph}\mathcal{L}[\sigma_p]\rho + \Gamma_2^{\rm ph}(\sigma_{++}\rho\sigma_{--} + \sigma_{--}\rho\sigma_{++}),
\end{aligned} \tag{B1}$$

where $\sigma_p = \sigma_{++} - \sigma_{--}$ and the parameters are defined as

$$\begin{aligned}
&\Gamma_{++} = \gamma_{ff}c^4, \quad \Gamma_{--} = \gamma_{ff}s^4, \quad \Gamma_{ee} = \gamma_{ee},\\
&\Gamma_{-+} = \gamma_{fg}s^4 + \gamma_{ff}c^2s^2, \quad \Gamma_{+-} = \gamma_{fg}c^4 + \gamma_{ff}c^2s^2,\\
&\Gamma_{e+} = \gamma_{eg}s^2, \quad \Gamma_{+e} = \gamma_{fe}c^2,\\
&\Gamma_{e-} = \gamma_{eg}c^2, \quad \Gamma_{-e} = \gamma_{fe}s^2,\\
&\Gamma_1^{\rm in} = \gamma_{eg}cs, \quad \Gamma_2^{\rm in} = \gamma_{fe}cs,\\
&\Gamma_1^{\rm ph} = \gamma_{fg}c^2s^2, \quad \Gamma_2^{\rm ph} = \gamma_{ff}c^2s^2.
\end{aligned} \tag{B2}$$

Here Γ_{ij} $(i, j = +, e, -,$ and $i \neq j)$ describe the incoherent population transfer between different dressed states, $\Gamma_k^{\rm ph}$ $(k = 1, 2)$ are the phase damping terms, and $\Gamma_k^{\rm in}$ $(k = 1, 2)$ represent the cross correlations between the incoherent processes $|e\rangle \to |\pm\rangle$ and $|\mp\rangle \to |e\rangle$. Starting from the master equation, we obtain

$$\begin{aligned}
\dot{\rho}_{++} &= -(\Gamma_{+e} + \Gamma_{+-})\rho_{++} + \Gamma_{-+}\rho_{--} + \Gamma_{e+}\rho_{ee},\\
\dot{\rho}_{--} &= \Gamma_{+-}\rho_{++} - (\Gamma_{-e} + \Gamma_{-+})\rho_{--} + \Gamma_{e-}\rho_{ee},
\end{aligned} \tag{B3}$$

where the dressed-state population satisfies the closed relation $\rho_{++} + \rho_{--} + \rho_{ee} = 1$. Here the effect of the cavity and magnon is temperately ignored as their coupling strengths are negligible compared to the driving field. Thus, the dressed populations are given by

$$\begin{aligned}
\rho_{++} &= \frac{1}{M}[s^2\gamma_{eg}(s^2\gamma_{fe} + s^2\gamma_{fg} + c^2\gamma_{ff})],\\
\rho_{--} &= \frac{1}{M}[c^2\gamma_{eg}(c^2\gamma_{fe} + c^2\gamma_{fg} + s^2\gamma_{ff})],\\
\rho_{ee} &= \frac{1}{M}[c^2s^2\gamma_{fe}(\gamma_{fe} + \gamma_{fg} + \gamma_{ff})],
\end{aligned} \tag{B4}$$

with $M = c^2s^2\gamma_{fe}(\gamma_{fe} + \gamma_{fg} + \gamma_{ff}) + \gamma_{eg}[(c^4 + s^4)(\gamma_{fe} + \gamma_{fg}) + 2c^2s^2\gamma_{ff}]$. For $\Delta_f = 0$, $s = c = 1/\sqrt{2}$, Eq. (B4) can be simplified as

$$\begin{aligned}
\rho_{++} = \rho_{--} &= \frac{\gamma_{eg}/\gamma_{fe}}{1 + 2\gamma_{eg}/\gamma_{fe}},\\
\rho_{ee} &= \frac{1}{1 + 2\gamma_{eg}/\gamma_{fe}}.
\end{aligned} \tag{B5}$$

[1] C. S. Muñoz, E. del Valle, A. G. Tudela, K. Müller, S. Lichtmannecker, M. Kaniber, C. Tejedor, J. J. Finley, and F. P. Laussy, Emitters of N-photon bundles, Nat. Photonics **8**, 550 (2014).

[2] J. C. López Carreño, C. Sánchez Muñoz, D. Sanvitto, E. del Valle, and F. P. Laussy, Exciting polaritons with quantum light, Phys. Rev. Lett. **115**, 196402 (2015).

[3] K. E. Dorfman, F. Schlawin, and S. Mukamel, Nonlinear optical signals and spectroscopy with quantum light, Rev. Mod. Phys. **88**, 045008 (2016).

[4] B. Bell, S. Kannan, A. McMillan, A. S. Clark, W. J. Wadsworth, and J. G. Rarity, Multicolor quantum metrology with entangled photons, Phys. Rev. Lett. **111**, 093603 (2013).

[5] W. Denk, J. H. Strickler, and W. W. Webb, Two-photon laser scanning fluorescence microscopy, Science **248**, 73 (1990).

[6] N. G. Horton, K. Wang, D. Kobat, C. G. Clark, F. W. Wise, C. B. Schaffer, and C. Xu, In *vivo* three-photon microscopy of subcortical structures of an intact mouse brain, Nat. Photonics **7**, 205 (2013).

[7] P. Lesani, G. Singh, C. M. Viray, Y. Ramaswamy, D. M. Zhu, P. Kingshott, Z. F. Lu, and H. Zreiqat, Two-photon dual-emissive carbon dot-based probe: deep-tissue imaging and ultrasensitive sensing of intracellular ferric ions, ACS Appl. Mater. Interfaces **12**, 18395 (2020).

[8] Y. W. Chu, P. Kharel, T. Yoon, L. Frunzio, P. T. Rakich, and R. J. Schoelkopf, Creation and control of multi-phonon fock

states in a bulk acoustic-wave resonator, Nature (London) **563**, 666 (2018).

[9] D. J. Gauthier, Q. L. Wu, S. E. Morin, and T. W. Mossberg, Realization of a continuous-wave, two-photon optical, laser, Phys. Rev. Lett. **68**, 464 (1992).

[10] C. Sánchez Muñoz, F. P. Laussy, E. del Valle, C. Tejedor, and A. González-Tudela, Filtering multiphoton emission from state-of-the-art cavity quantum electrodynamics, Optica **5**, 14 (2018).

[11] Q. Bin, Y. Wu, and X.-Y. Lü, Parity-symmetry-protected multiphoton bundle emission, Phys. Rev. Lett. **127**, 073602 (2021).

[12] Q. Bin, X.-Y. Lü, F. P. Laussy, F. Nori, and Y. Wu, N-phonon bundle emission via the stokes process, Phys. Rev. Lett. **124**, 053601 (2020).

[13] F. Zou, J.-Q. Liao, and Y. Li, Dynamical emission of phonon pairs in optomechanical systems, Phys. Rev. A **105**, 053507 (2022).

[14] C. Gou, X. Hu, and F. Wang, Antibunched two-mode two-photon bundles via atomic coherence, Phys. Rev. A **106**, 063718 (2022).

[15] S.-Y. Jiang, F. Zou, Y. Wang, J.-F. Huang, X.-W. Xu, and J.-Q. Liao, Multiple-photon bundle emission in the n-photon Jaynes-Cummings model, Opt. Express **31**, 15697 (2023).

[16] C. Liu, J.-F. Huang, and L. Tian, Deterministic generation of multi-photon bundles in a quantum Rabi model, Sci. China: Phys., Mech. Astron. **66**, 220311 (2023).

[17] Y. Chang, A. González-Tudela, C. S. Muñoz, C. Navarrete-Benlloch, and T. Shi, Deterministic down-converter and continuous photon-pair source within the bad-cavity limit, Phys. Rev. Lett. **117**, 203602 (2016).

[18] S.-L. Ma, X.-K. Li, Y.-L. Ren, J.-K. Xie, and F.-L. Li, Antibunched N-photon bundles emitted by a Josephson photonic device, Phys. Rev. Res. **3**, 043020 (2021).

[19] S.-L. Ma, J.-K. Xie, Y.-L. Ren, X.-K. Li, and F.-L. Li, Photon-pair blockade in a josephson-photonics circuit with two nondegenerate microwave resonators, New J. Phys. **24**, 053001 (2022).

[20] M. Cosacchi, A. Mielnik-Pyszczorski, T. Seidelmann, M. Cygorek, A. Vagov, D. E. Reiter, and V. M. Axt, N-photon bundle statistics in different solid-state platforms, Phys. Rev. B **106**, 115304 (2022).

[21] F. Zou, Y. Li and J.-Q. Liao, Dynamical N-photon bundle emission, New J. Phys. **25**, 043027 (2023).

[22] C. Sánchez Muñoz, F. P. Laussy, C. Tejedor, and E. del Valle, Enhanced two-photon emission from a dressed biexciton, New J. Phys. **17**, 123021 (2015).

[23] Y. Deng, T. Shi, and S. Yi, Motional n-phonon bundle states of a trapped atom with clock transitions, Photonics Res. **9**, 1289 (2021).

[24] A. González-Tudela, V. Paulisch, H. J. Kimble, and J. I. Cirac, Efficient multiphoton generation in waveguide quantum electrodynamics, Phys. Rev. Lett. **118**, 213601 (2017).

[25] H. Y. Yuan, J. K. Xie, and R. A. Duine, Magnon bundle in a strongly dissipative magnet, Phys. Rev. Appl. **19**, 064070 (2023).

[26] C. Kittel, *Introduction to Solid State Physics* (Wiley, Hoboken, NJ, 1966).

[27] S. O. Demokritov, B. Hillebrands, and A. N. Slavin, Brillouin light scattering studies of confined spin waves: Linear and nonlinear confinement, Phys. Rep. **348**, 441 (2001).

[28] B. Z. Rameshti, S. V. Kusminskiy, J. A. Haigh, K. Usami, D. Lachance-Quirion, Y. Nakamura, C.-M. Hu, H. X. Tang, G. E. W. Bauer, and Y. M. Blanter, Cavity magnonics, Phys. Rep. **979**, 1 (2022).

[29] D. Lachance-Quirion, Y. Tabuchi, A. Gloppe, K. Usami, and Y. Nakamura, Hybrid quantum systems based on magnonics, Appl. Phys. Express **12**, 070101 (2019).

[30] Y. Kajiwara, K. Harii, S. Takahashi, J. Ohe, K. Uchida, M. Mizuguchi, H. Umezawa, H. Kawai, K. Ando, K. Takanashi, S. Maekawa, and E. Saitoh, Transmission of electrical signals by spinwave interconversion in a magnetic insulator, Nature (London) **464**, 262 (2010).

[31] C. Liu, J. Chen, T. Liu, F. Heimbach, H. Yu, Y. Xiao, J. Hu, M. Liu, H. Chang, T. Stueckler, S. Tu, Y. Zhang, Y. Zhang, P. Gao, Z. Liao, D. Yu, K. Xia, N. Lei, W. Zhao, and M. Wu, Long-distance propagation of short-wavelength spin waves, Nat. Commun. **9**, 738 (2018).

[32] Y.-X. Liu, J. Q. You, L. F. Wei, C. P. Sun, and F. Nori, Optical selection rules and phase-dependent adiabatic state control in a superconducting quantum circuit, Phys. Rev. Lett. **95**, 087001 (2005).

[33] Y. Tabuchi, S. Ishino, A. Noguchi, T. Ishikawa, R. Yamazaki, K. Usami, and Y. Nakamura, Coherent coupling between a ferromagnetic magnon and a superconducting qubit, Science **349**, 405 (2015).

[34] C. Kittel, On the theory of ferromagnetic resonance absorption, Phys. Rev. **73**, 155 (1948).

[35] T. Holstein and H. Primakoff, Field dependence of the intrinsic domain magnetization of a ferromagnet, Phys. Rev. **58**, 1098 (1940).

[36] M. O. Scully and M. S. Zubairy, *Quantum Optics* (Cambridge University Press, Cambridge, England, 1997).

[37] D. F. Walls and G. J. Milburn, *Quantum Optics* (Springer, Berlin, 1994).

[38] J. R. Johansson, P. D. Nation, and F. Nori, QuTiP: An open-source Python framework for the dynamics of open quantum systems, Comput. Phys. Commun. **183**, 1760 (2012).

[39] C. Cohen-Tannoudji, J. Dupont-Roc, and G. Grynberg, *Atom-Photon Interactions* (Wiley, New York, 1992).

[40] B. R. Mollow, Power spectrum of light scattered by two-level systems, Phys. Rev. **188**, 1969 (1969).

[41] J. C. López Carreño, E. del Valle, and F. P. Laussy, Photon correlations from the Mollow triplet, Laser Photonics Rev. **11**, 1700090 (2017).

[42] R. J. Glauber, The quantum theory of optical coherence, Phys. Rev. **130**, 2529 (1963).

[43] Z. H. Peng, Y. Liu, J. T. Peltonen, T. Yamamoto, J. S. Tsai, and O. Astafiev, Correlated emission lasing in harmonic oscillators coupled via a single three-level artificial atom, Phys. Rev. Lett. **115**, 223603 (2015).

[44] F. Wang, W. Nie, X. Feng, and C. H. Oh, Steady-state entanglement of harmonic oscillators via dissipation in a single superconducting artificial atom, Phys. Rev. A **94**, 012330 (2016).

[45] A. Kuzmich, W. P. Bowen, A. D. Boozer, A. Boca, C. W. Chou, L.-M. Duan, and H. J. Kimble, Generation of nonclassical photon pairs for scalable quantum communication with atomic ensembles, Nature (London) **423**, 731 (2003).

[46] J. W. Rao, S. Kaur, B. M. Yao, E. R. J. Edwards, Y. T. Zhao, X. Fan, D. Xue, T. J. Silva, Y. S. Gui, and C. M. Hu, Analogue

of dynamic Hall effect in cavity magnon polariton system and coherently controlled logic device, Nat. Commun. **10**, 2934 (2019).

[47] Y. Yang, J. W. Rao, Y. S. Gui, B. M. Yao, W. Lu, and C.-M. Hu, Control of the magnon-photon level attraction in a planar cavity, Phys. Rev. Appl. **11**, 054023 (2019).

[48] H. Huebl, C. W. Zollitsch, J. Lotze, F. Hocke, M. Greifenstein, A. Marx, R. Gross, and S. T. B. Goennenwein, High cooperativity in coupled microwave resonator ferrimagnetic insulator hybrids, Phys. Rev. Lett. **111**, 127003 (2013).

[49] Y. Tabuchi, S. Ishino, T. Ishikawa, R. Yamazaki, K. Usami, and Y. Nakamura, Hybridizing ferromagnetic magnons and microwave photons in the quantum limit, Phys. Rev. Lett. **113**, 083603 (2014).

[50] X. Zhang, C.-L. Zou, L. Jiang, and H. X. Tang, Strongly coupled magnons and cavity microwave photons, Phys. Rev. Lett. **113**, 156401 (2014).

[51] M. Goryachev, W. G. Farr, D. L. Creedon, Y. Fan, M. Kostylev, and M. E. Tobar, High-cooperativity cavity QED with magnons at microwave frequencies, Phys. Rev. Appl. **2**, 054002 (2014).

[52] L. Bai, M. Harder, Y.-P. Chen, X. Fan, J.-Q. Xiao, and C.-M. Hu, Spin pumping in electrodynamically coupled magnon-photon systems, Phys. Rev. Lett. **114**, 227201 (2015).

[53] D. K. Zhang, X.-M. Wang, T.-F. Li, X.-Q. Luo, W. D. Wu, F. Nori, and J. Q. You, Cavity quantum electrodynamics with ferromagnetic magnons in a small yttrium-iron-garnet sphere, npj Quantum Inf. **1**, 15014 (2015).

[54] J. Bourhill, N. Kostylev, M. Goryachev, D. L. Creedon, and M. E. Tobar, Ultrahigh cooperativity interactions between magnons and resonant photons in a YIG sphere, Phys. Rev. B **93**, 144420 (2016).

[55] N. Kostylev, M. Goryachev, and M. E. Tobar, Superstrong coupling of a microwave cavity to yttrium iron garnet magnons, Appl. Phys. Lett. **108**, 062402 (2016).

[56] Y. Tabuchi, S. Ishino, A. Noguchi, T. Ishikawa, R. Yamazaki, K. Usami, and Y. Nakamura, Quantum magnonics: The magnon meets the superconducting qubit, C. R. Phys. **17**, 729 (2016).

[57] K. Wu, W. Zhong, G. Cheng, and A. Chen, Phase-controlled multimagnon blockade and magnon-induced tunneling in a hybrid superconducting system, Phys. Rev. A **103**, 052411 (2021).

[58] D. Kong, X. Hu, L. Hu, and J. Xu, Magnon-atom interaction via dispersive cavities: Magnon entanglement, Phys. Rev. B **103**, 224416 (2021).

[59] D. Kong, J. Xu, Y. Tian, F. Wang, and X. Hu, Remote asymmetric einstein-podolsky-rosen steering of magnons via a single pathway of Bogoliubov dissipation, Phys. Rev. Res. **4**, 013084 (2022).

[60] D. Kong, J. Xu, C. Gong, F. Wang, and X. Hu, Magnon-atom-optical photon entanglement via the microwave photon-mediated Raman interaction, Opt. Express **30**, 34998 (2022).

[61] F. Wang, C. Gou, J. Xu, and C. Gong, Hybrid magnon-atom entanglement and magnon blockade via quantum interference, Phys. Rev. A **106**, 013705 (2022).

[62] F. Wang and C. Gou, Magnon-induced absorption via quantum interference, Opt. Lett. **48**, 1164 (2023).

[63] T. Hioki, H. Shimizu, T. Makiuchi, and E. Saitoh, State tomography for magnetization dynamics, Phys. Rev. B **104**, L100419 (2021).

[64] D. Xu, X.-K. Gu, H.-K. Li, Y.-C. Weng, Y.-P. Wang, J. Li, H. Wang, S.-Y. Zhu, and J. Q. You, Quantum control of a single magnon in a macroscopic spin system, Phys. Rev. Lett. **130**, 193603 (2023).

[65] D. Lachance-Quirion, Y. Tabuchi, S. Ishino, A. Noguchi, T. Ishikawa, R. Yamazaki, and Y. Nakamura, Resolving quanta of collective spin excitations in a millimeter-sized ferromagnet, Sci. Adv. **3**, e1603150 (2017).

[66] D. Lachance-Quirion, S. P. Wolski, Y. Tabuchi, S. Kono, K. Usami, and Y. Nakamura, Entanglement-based single-shot detection of a single magnon with a superconducting qubit, Science **367**, 425 (2020).